

C. Bonadonna · B. F. Houghton

## Total grain-size distribution and volume of tephra-fall deposits

Received: 27 January 2004 / Accepted: 19 August 2004 / Published online: 26 January 2005  
© Springer-Verlag 2005

**Abstract** On 17 June 1996, Ruapehu volcano, New Zealand, produced a sustained andesitic sub-Plinian eruption, which generated a narrow tephra-fall deposit extending more than 200 km from the volcano. The extremely detailed data set from this eruption allowed methods for the determination of total grain-size distribution and volume of tephra-fall deposits to be critically investigated. Calculated total grain-size distributions of tephra-fall deposits depend strongly on the method used and on the availability of data across the entire dispersal area. The Voronoi Tessellation method was tested for the Ruapehu deposit and gave the best results when applied to a data set extending out to isomass values of  $<1 \text{ g m}^{-2}$ . The total grain-size distribution of a deposit is also strongly influenced by the very proximal samples, and this can be shown by artificially constructing subsets from the Ruapehu database. Unless the available data set is large, all existing techniques for calculations of total grain-size distribution give only apparent distributions. The tephra-fall deposit from Ruapehu does not show a simple exponential thinning, but can be approximated well by at least three straight-line segments or by a power-law fit on semi-log plots of thickness vs. (area)<sup>1/2</sup>. Integrations of both fits give similar volumes of about  $4 \times 10^6 \text{ m}^3$ . Integration of at least three exponential segments and of a power-law fit with at least ten isopach contours available can be considered as a good estimate

of the actual volume of tephra fall. Integrations of smaller data sets are more problematic.

**Keywords** Tephra-fall deposits · Voronoi · Ruapehu · Exponential thinning · Power-law thinning

### Introduction

On 17 June 1996, Ruapehu volcano, New Zealand, produced a prolonged andesitic sub-Plinian eruption characterised by two sustained plumes about 2 h apart that reached a maximum height of 8.5 km above sea level (Prata and Grant 2001). These two plumes were affected by a strong SSW wind ( $15\text{--}35 \text{ m s}^{-1}$ , Prata and Grant 2001) and generated a narrow tephra-fall deposit extending more than 200 km from the volcano (Cronin et al. 1998; Hurst and Turner 1999). This was one of several sub-Plinian eruptions from Ruapehu in 1995 and 1996, but external factors led to an unusually complete record of the deposit. Firstly, the eruption took place during a long period of stable dry weather, so that the very distal parts of the tephra-fall deposit could be sampled over the following 7 days. Secondly, a southerly wind meant that the deposit was dispersed on the flat-lying northern summit plateau of Ruapehu, at a time when the winter snow pack was actively accumulating. Very proximal deposits fell on fresh snow and was immediately buried by further snowfall. This preserved the beds, to within 200 m of vent, in a completely undisturbed state. The very complete data set from this eruption (mass per unit area values ranging from about 3,000 to  $0.0002 \text{ kg m}^{-2}$  for samples collected between 0.2 and 200 km downwind from the vent) provides an unusual opportunity to re-evaluate methods for estimating total grain-size distribution and deposit volumes. Field data and grain-size analysis used here are from Houghton et al. (1996, unpublished data). In the rest of the paper we will use the term 'Ruapehu' to indicate features associated with the tephra-fall deposit generated by the 17 June 1996 eruptive event of Ruapehu volcano.

The total grain-size distribution of pyroclastic deposits is often poorly constrained due to the sparse data and to

Editorial responsibility: H. Shinohara

C. Bonadonna  
Department of Earth Sciences,  
University of Bristol,  
Bristol, BS8 1RJ, UK

C. Bonadonna (✉) · B. F. Houghton  
Department of Geology and Geophysics,  
University of Hawaii,  
1680 East-West Road, POST Building 617a, Honolulu,  
HI 96822, USA  
e-mail: costanza@hawaii.edu  
Tel.: +1-808-9565033  
Fax: +1-808-9565512

inconsistencies in the methods used. Different methods have been used in the past for different deposits (e.g. Walker 1980; Carey and Sigurdsson 1982), but the lack of a standard approach makes the comparison of these data difficult. The use of a well-known and reliable statistical tool known as Voronoi tessellation (e.g. Okabe et al. 1992) is here suggested and tested against the Ruapehu data. The limitations of calculations based on partial data are also investigated by artificially constructing smaller data sets that are either uniformly distributed across the dispersal area or lacking in samples from either proximal or distal environments.

The large Ruapehu data set is also useful to investigate methods of calculating the volumes of tephra fall, another parameter crucial to the understanding and characterisation of an eruption, but in practice often very difficult to determine. Several methods have been suggested to interpolate and/or extrapolate available data and the most recent ones assume an exponential decay of thickness with distance from vent (Pyle 1989; Fierstein and Nathenson 1992). However, real thickness trends are still not well understood. Many field data appear to fit an exponential decay model (e.g. Pyle 1989), but they can also be described by a power-law trend (e.g. Bonadonna et al. 1998). It is also evident now that most deposits are not described by a *simple exponential thinning*, but show at least two segments on semi-log plots of thickness vs (area)<sup>1/2</sup> (Pyle 1990; Fierstein and Nathenson 1992; Pyle 1995; Bonadonna and Phillips 2003). A *simple exponential thinning* is considered here as described by only one straight-line segment on a semi-log plot of thickness vs (area)<sup>1/2</sup>. Therefore, the current use of methods for volume calculations may still either underestimate or overestimate the deposit volume (Pyle 1990; Pyle 1995; Bonadonna et al. 1998). A new method of volume calculation by integration of the power-law fit is presented here and compared with existing techniques and, in particular, with the exponential approach.

### Calculations of total grain-size distribution

Total grain-size distribution of tephra-fall deposits is a crucial eruptive parameter. Firstly, it can be used to infer fragmentation and eruption style by linking particle size to the initial gas content and water–magma interaction processes (e.g. Houghton and Wilson 1998; Kaminski and Jaupart 1998). Second, it is an important constraint for sedimentation models that help understand plume dynamics (e.g. Bursik et al. 1992; Sparks et al. 1992). Third, it is necessary for hazard mitigation plans as it is used in tephra-dispersal modelling to assess the risk and vulnerability of populations (e.g. Barberi et al. 1990; Connor et al. 2001; Bonadonna et al. 2002a) and because it is an important indication of the level of particulate pollution dangerous for human health (e.g. Moore et al. 2002). Unfortunately, the determination of total grain-size distributions presents several difficulties due to (1) methodological problems related to the integration of

grain-size analysis of single samples, (2) scarcity of data points and (3) uneven data-point distribution.

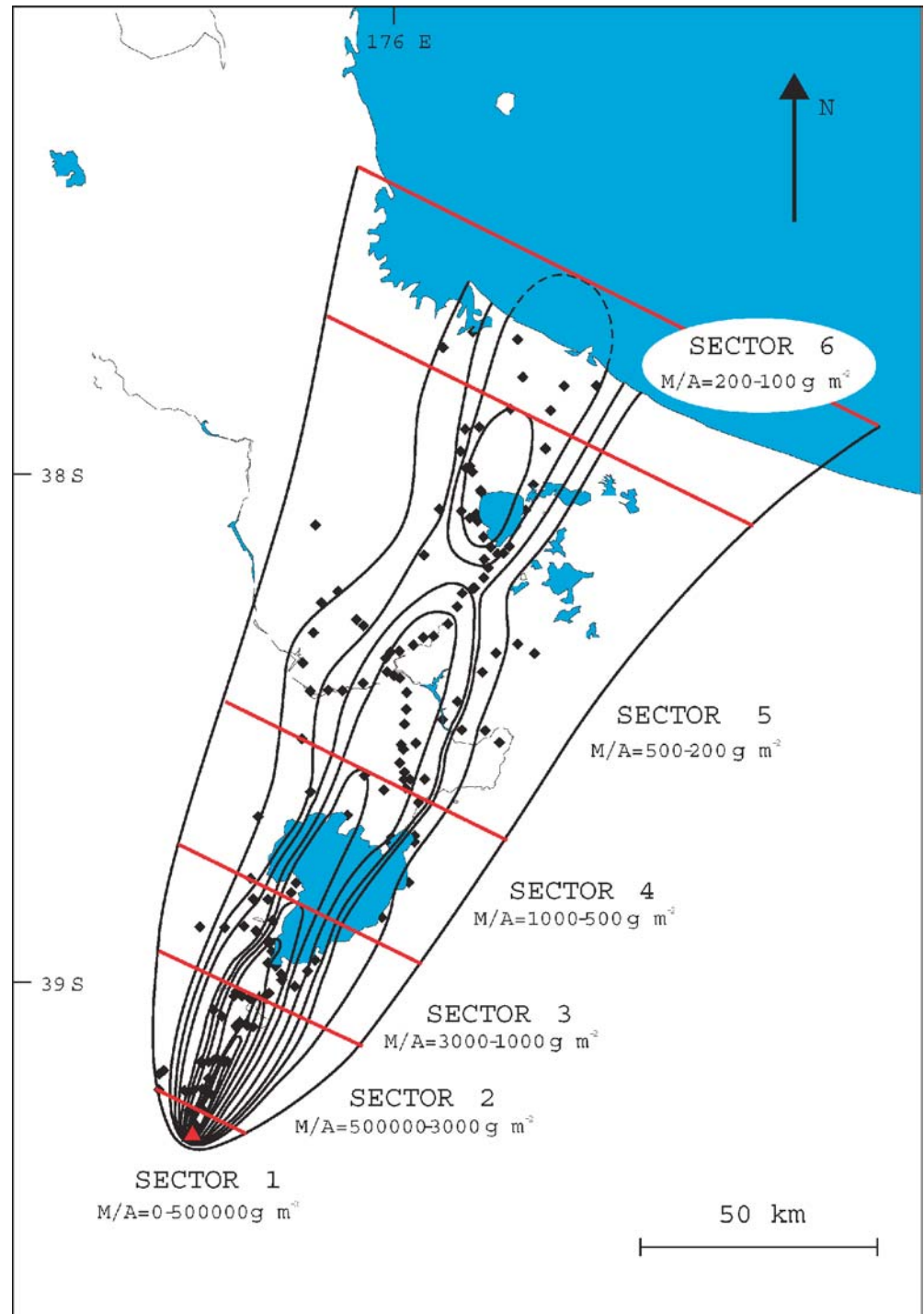
Many grain-size analyses carried out for tephra-fall deposits are incomplete, lacking data below 63  $\mu\text{m}$  (i.e.  $4\phi$ , with  $\phi = -\log_2 d$ , where  $d$  is the particle diameter in mm; e.g. Walker 1980, 1981c). Commonly, a scarcity of samples also makes the reconstruction of the total grain-size distribution difficult and the result becomes very dependent on the calculation method used. The calculation of total grain-size distributions may be biased against either or both the very coarse or very fine size populations because very proximal and very distal samples are commonly not available for analysis. For future eruptions, satellite studies may be used to deal with missing data in the distal area by retrieval of size data using AVHRR bands 4 and 5 (Wen and Rose 1994). This technique has the advantage that it can detect very fine particles that are suspended for long periods in the atmosphere or can be easily eroded away due to their very small diameter. But retrieval of particle sizes using this technique can only resolve those particles with effective radii  $<10 \mu\text{m}$ .

### Grain-size-calculation techniques

Several techniques have been utilised to determine the total grain-size distribution of a tephra-fall deposit. Only a few workers have attempted to synthesise data sets from individual samples: approaches have ranged from a simple unweighted averaging of all available grain-size analyses, e.g. Rotongaio ash (Walker 1981a), to various step-wise integrations of data that may be weighted either by deposit thickness or mass. Walker (1980, 1981a, 1981c) prepared isomass maps for each grain-size class for four deposits at Taupo and integrated these data to get the total mass for each size class, which could then be summed to derive a total deposit grain size. Murrow et al. (1980) calculated average grain-size distribution for the regions enclosed by each grain-size isopach and then weighted that data with respect to the enclosed volume to arrive at the total grain-size distribution. Sparks et al. (1981) divided the isopach map of the 1875 Askja Plinian fall into segments and integrated grain-size data weighted by enclosed volume. Carey and Sigurdsson (1982) integrated data for the 18 May 1980, Mount St Helens tephra-fall deposit by dividing the dispersal area into a series of 13 polygons and calculating the total mass within each polygon and the average grain size of all samples from within the polygon. They then weighted the latter by the former to arrive at a total grain-size distribution. Parfitt (1998) calculated average grain-size distributions for the regions between each pair of isopachs for the Kilauea Iki 1959 tephra-fall deposit and then combined these data with volume estimates and clast density data to derive the total mass of material in each size class for each zone.

The Ruapehu data set is large enough to allow different total grain-size calculation methods to be investigated. Three different techniques are compared here. In technique A, the weighted average of sample grain-size

**Fig. 1** Isomass map from Houghton et al. (1996, unpublished data), showing the 'sectorisation' (red lines) of the Ruapehu deposit used to calculate the total grain-size distribution (technique B). The mass per unit area ( $M/A$ ) characteristic for each sector is also indicated. The most external line represents the isoline of zero mass compiled from field observations. The dashed line indicates extrapolation of land data to the sea, the red triangle indicates the position of the volcano and the black diamonds indicate the sample points used in the calculations



distribution for all samples over the whole deposit is calculated. Each data set is weighted by the mass per unit area value for that site (Houghton et al. 1996, unpublished data). For technique B, a variation of the Carey and Sigurdsson (1982) approach is considered, by dividing the tephra-fall deposit into arbitrary sectors and weighting the sample grain-size distribution over each sector. The sectoral grain-size distribution is then weighted again over the whole deposit (Fig. 1). In technique C, the Voronoi tessellation statistical method is used. The Voronoi tes-

sellation is a well-known method of spatial analysis and can be defined as the partitioning of the plane such that, for any set of distinct data points, the cell associated with a particular data point contains all spatial locations closer to that point than to any other (e.g. Okabe et al. 1992).

The Voronoi tessellation is commonly used in applied sciences (e.g. Nelson 1979; Jasny 1988; Haydon and Piana 1999; Wilkinson et al. 1999; Bohm et al. 2000; Duyckaerts and Godefroy 2000; Zhan and Troy 2000; Blower et al. 2003; Dupuis et al. 2004), but because this is



**Fig. 2** Map showing the Voronoi tessellation applied to the Ruapehu deposit to calculate the total grain-size distribution (technique C). Each polygon represents a Voronoi cell built for each sample point (black circles), and is assigned with the same mass per unit area values and grain-size distributions as the corresponding sample points. The most external line represents the isoline of zero mass in Fig. 1. The thin line indicates the NE coast of New Zealand. All polygons outside the zero line and in the ocean are given mass zero (corresponding to the blue crosses)

the first time this method has been applied to a pyroclastic deposit, it is here described in detail. An edge (say between sample point  $SP_1$  and sample point  $SP_2$ ) of a Voronoi cell is a line segment that is a subset of the perpendicular bisector of the line segment connecting  $SP_1$  and  $SP_2$ . The mass per unit area value and the grain-size distribution of each sample point  $SP_1$ ,  $SP_2$ ,  $SP_3$ , etc. ..., are assigned to the enclosing Voronoi cells  $VC_1$ ,  $VC_2$ ,  $VC_3$ , etc. ... As a conclusion, the tephra-fall deposit is divided into Voronoi cells whose interior consists of all grid points, which are closer to a particular sample point than to any other (Fig. 2). Then the total grain-size distribution is obtained as the area-weighted average of all the Voronoi cells over the whole deposit.

There are hundreds of different algorithms for constructing various types of Voronoi diagrams (e.g. Brown 1979; Gowda et al. 1983; Klein 1989). We have compiled a MatLab code that uses the Delaunay triangulation to assign a Voronoi cell to each sample point considered and determines the total grain-size distribution of the corre-

sponding tephra-fall deposit (<http://www.soest.hawaii.edu/IAVCEI-tephra-group/grainsize.htm>).

### The influence of different grain-size-calculation techniques

Grain-size distributions obtained by techniques A, B and C all show two main subpopulations with a slight saddle at  $-1\phi$  (Fig. 3). However, the weight fractions and the modes of these two subpopulations vary significantly. Techniques A and C give grain-size distributions that can be approximated by a Gaussian distribution with mode at about  $-0.8\phi$ , with about 99.9 wt% of particles between 256  $\mu\text{m}$  and 1  $\mu\text{m}$  ( $-8$  to  $10\phi$ ). However, two lognormal subpopulations could also be identified by using the Sequential Fragmentation/Transport Analysis Windows application described in Wohletz et al. (1989) with modes at about  $-2\phi$  and  $0\phi$ , respectively. Corresponding proportions for each mode are 50 wt% for both subpopulations resulting from technique A, and 40 and 60 wt% for the two main lognormal subpopulations resulting from technique C. Technique B generates a grain-size distribution with two subpopulations with modes at  $-2.5\phi$  and  $2\phi$  and mode proportions of 25 and 75 wt%, respectively. All distributions also show a third minor subpopulation with mode at  $-7\phi$  with wt% <2. The Inmann graphical statistical parameters (Inman 1952) for the grain-size distributions resulting from the three techniques described above are shown in Table 1.

Techniques A and C give similar results because in both cases samples are weighted over the whole deposit without introducing any biasing factor (Fig. 3 and Table 1). In contrast, the 'sectorisation' of the deposit (technique B) inevitably introduces some bias due to the choice of sectors. As an example, the grain-size distribution in Fig. 3b still shows two distinct subpopulations, but is clearly biased towards fine grain sizes due to the choice of large distal sectors (Fig. 1).

Sectorisation techniques have often been used to calculate total grain-size distribution with choices of sectors made according to the specific characteristics of different deposits (e.g. Sparks et al. 1981; Carey and Sigurdsson 1982; Parfitt 1998). This study indicates that this approach can be relatively unreliable. Techniques A and C provide a better statistical result that does not require any arbitrary choice of sectors. However, technique A could also introduce some bias in a case where the samples used for calculations are not uniformly distributed. This is the reason why some authors have used several variations of technique B, to permit some weighting allowance for uneven distributions of samples. Technique C aims to provide a compromise between techniques A and B, as it partitions the deposit into polygons that weight the data without introducing any subjective bias, as the polygons are the result of a geometrical construction that entirely depends on the sample distribution. Given the state of the art in terms of grain-size calculations, Voronoi tessellation is suggested as an alternative statistical method to determine the total grain-size distribution.

**Fig. 3** Whole deposit grain-size distribution for the Ruapehu deposit obtained by using **a** technique A, **b** technique B and **c** technique C.  $\phi = -\log_2(d)$ , where  $d$  is the particle diameter in mm

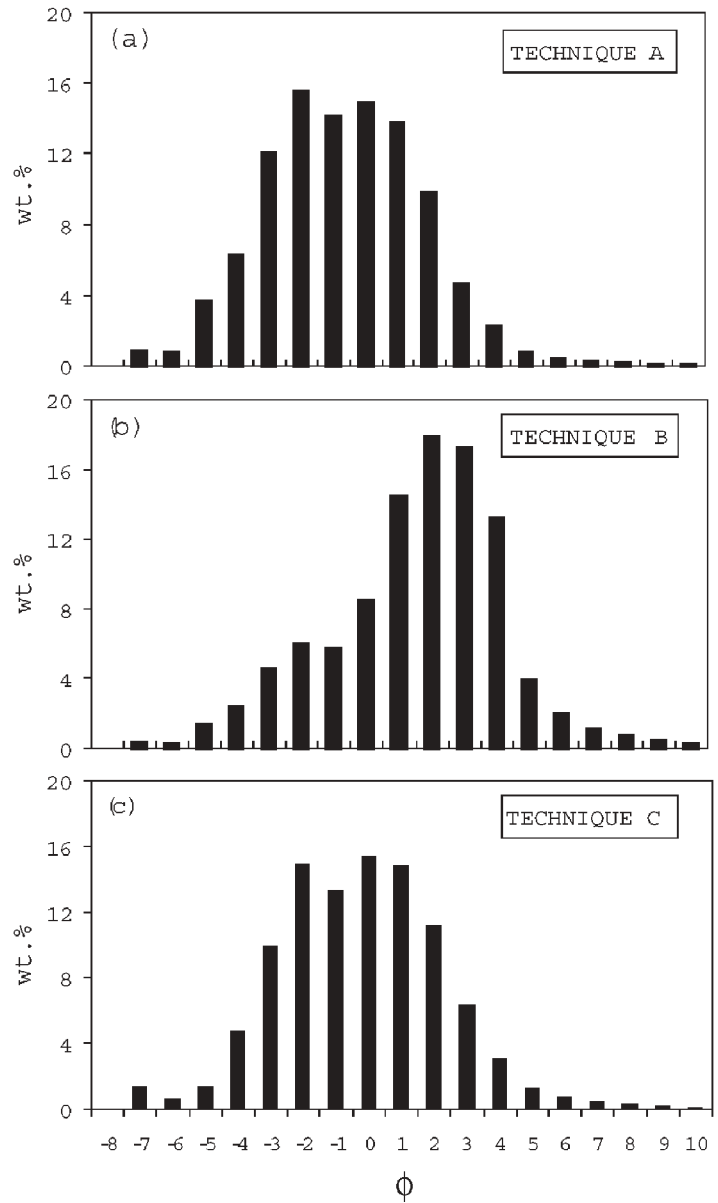


**Table 1** Inman graphical statistical parameters for the grain-size distributions determined with techniques A, B and C in Fig. 3 and for the data sets 2–6 in Fig. 5. Data set 1 is not shown in this table because it is equivalent to technique C.  $Md_\phi$  is the median diameter,  $\sigma_\phi$  is the graphic standard deviation and SkG is the graphic skewness (Inman 1952).  $\phi = -\log_2(d)$ , where  $d$  is the particle diameter in mm

	$Md_\phi(\phi)$	$\sigma_\phi$	SkG
Technique A	-1.25	2.40	0.00
Technique B	1.35	2.58	-0.22
Technique C	-0.80	2.43	-0.01
Data set 2	0.05	2.18	0.01
Data set 3	0.10	2.18	0.26
Data set 4	1.55	1.60	0.09
Data set 5	2.55	1.33	0.13
Data set 6	2.80	1.18	0.23

#### The influence of the availability of data

The data set from the Ruapehu deposit is unusually complete for both distal and very proximal locations. By selecting only subsets of these data, the sensitivity of calculated total grain-size distribution to the quality of data sets can be evaluated. In this test, six different data sets are considered as follows:

- Data set 1: the original complete data set (Fig. 4a).
- Data set 2: data set 1 reduced to about 50%, but preserving a uniform distribution across the total outcrop area (Fig. 4b).
- Data set 3: data set 1 reduced to about 10%, but preserving a uniform distribution across the total outcrop area (Fig. 4c).

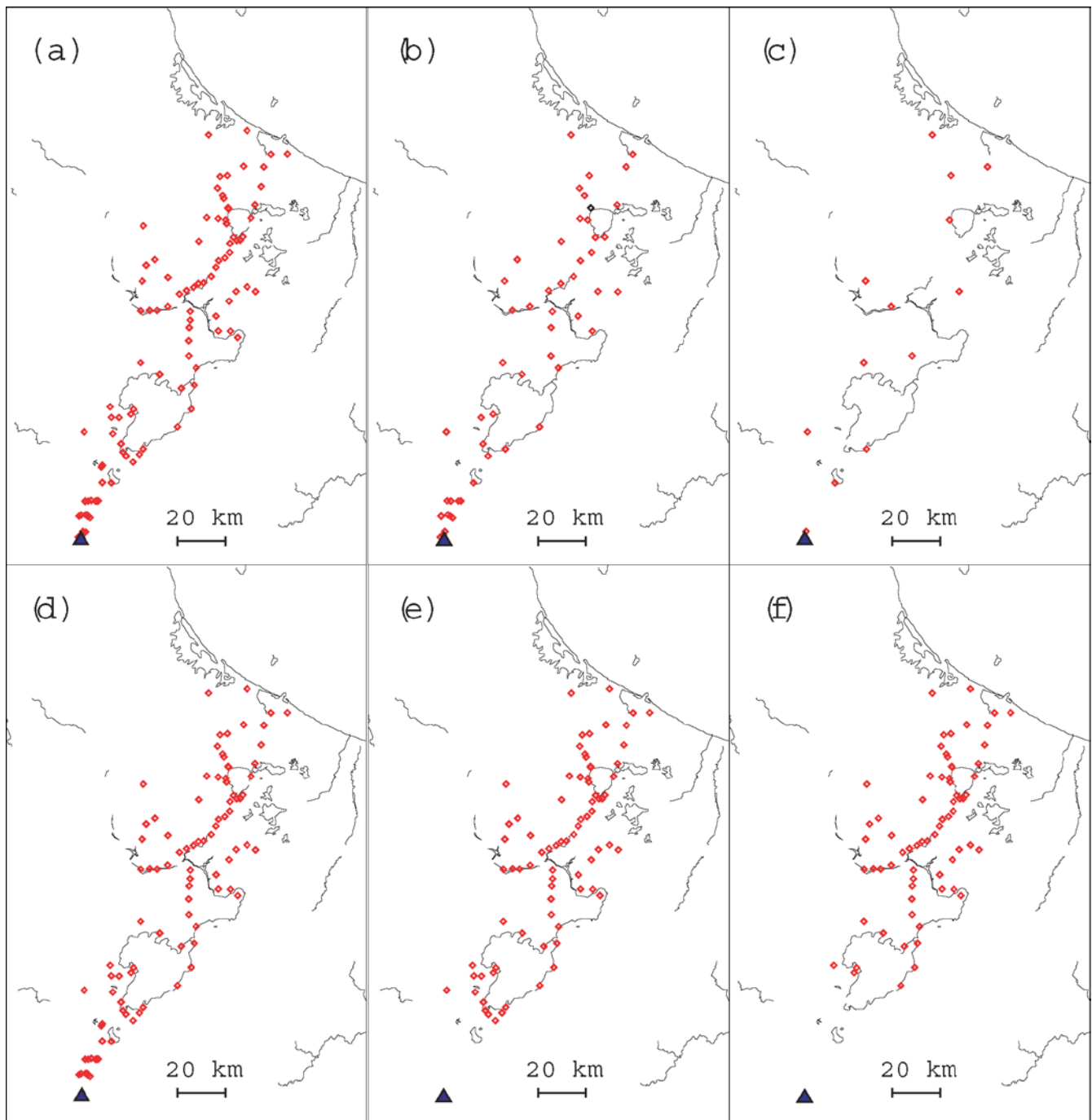


**Fig. 4** Data sets used to assess the influence of the availability of data. **a** Data set 1 (complete data set), **b** data set 2 (data set 1 reduced to about 50% preserving a uniform distribution), **c** data set 3 (data set 1 reduced to about 10% preserving a uniform distribution), **d** data set 4 [data set 1 reduced to about 90% by eliminating

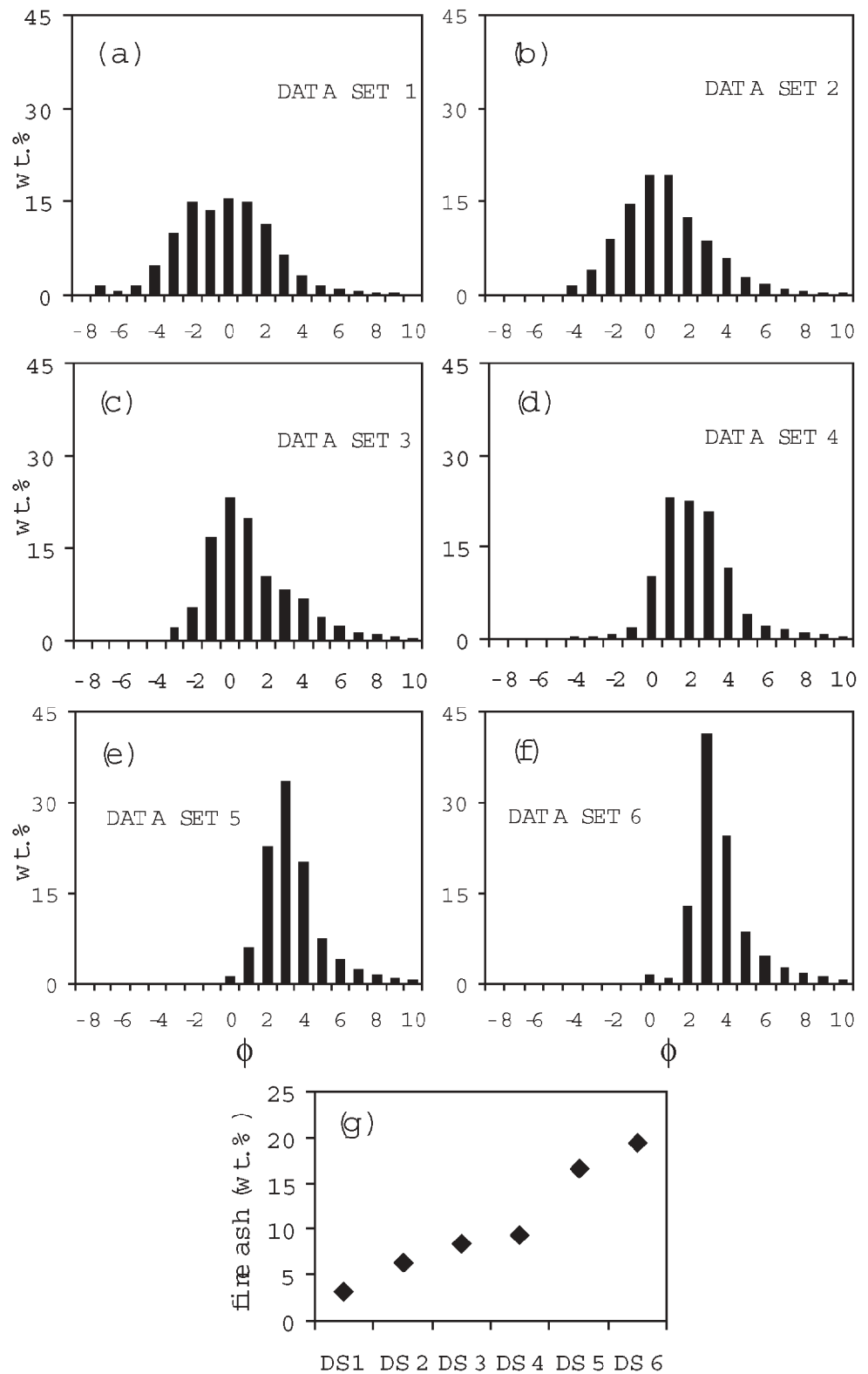
very proximal (0–5 km) samples], **e** data set 5 [data set 1 reduced to about 70% by eliminating proximal (0–30 km) samples], and **f** data set 6 [data set 1 reduced to about 60% by eliminating proximal and medial (0–50 km) samples]. Red diamonds and blue triangle indicate sample points and eruptive vent, respectively

- Data set 4: data set 1 reduced to about 90% by eliminating very proximal samples (i.e. samples within 5 km from the vent) (Fig. 4d).
- Data set 5: data set 1 reduced to about 70% by eliminating all samples up to 30 km from the vent (Fig. 4e).
- Data set 6: data set 1 reduced to about 60% by eliminating all samples up to 50 km from the vent (Fig. 4f).

Data sets 2 and 3 simulate a deposit with rather limited but uniform exposure. Data sets 4 to 6 approximate to scenarios where the proximal and medial deposit is buried or obscured by vent collapse and/or is inaccessible to different extents.

Total grain-size distributions for data sets 1–6 were calculated by technique C. Figure 5 shows that the re-

**Fig. 5** Grain-size distributions obtained by applying technique C (i.e. Voronoi tessellation, in Fig. 2) to the different data subsets in Fig. 4. **a** Data set 1, **b** data set 2, **c** data set 3, **d** data set 4, **e** data set 5 and **f** data set 6. **g** shows the variation of the apparent fine-ash content (particles with diameter  $<63 \mu\text{m}$ ) for the six data subsets



sulting total grain-size distribution strongly depends on the data set considered and that it is strongly skewed by the most proximal samples available. Comparison between the total grain-size distribution calculated from data set 1 (complete data set; Fig. 4a) and data set 6 (most

distal samples; Fig. 4f) shows that availability of proximal samples are of critical importance (Fig 5a, f). This is because proximal samples have more weight in the calculations, being characterised by larger values of mass per unit area. Even total grain-size distributions calculated

using data sets 1, 2 and 3 (all uniformly distributed) show slightly different results (the former being slightly bimodal) with an apparent fining of the deposit as the number of samples decreases (Fig. 5g; Table 1).

Figures 5a, b show that technique C gives reasonable results also for a reduced but uniform data set, even though the resulting Inman parameters for data sets 1 and 2 show some differences (Table 1). If the data set is not uniform, and especially if proximal data are missing, technique C fails to give a good representation of the true grain size (Fig. 5d–f; Table 1). This suggests that, unless a uniformly distributed data set is available for a given tephra-fall deposit, any calculated total grain-size distribution will be an apparent total grain-size distribution, with the quality of data reflecting the availability of samples for that specific deposit. In order to obtain a total grain-size distribution that better represents the original distribution, a reliable extrapolation of data to proximal and distal area is needed.

As a conclusion, total grain-size distributions obtained from poor data sets lacking of either distal or proximal data tend to be problematic due to the issues discussed above. However, the sensitivity of the analysis also depends on the sorting of the initial particle distribution, which relates to the style and the intensity of a given eruption. As an example, co-PF deposits are typically characterised by particles with diameter  $<1$  mm and, therefore, would be less sensitive to the data sets analysed (e.g. Bonadonna et al. 2002b). Grain-size distributions of tephra-fall deposits from weak-plumes, such as the Ruapehu deposit, are more likely to be sensitive to the data sets analysed because they are characterised by poorly sorted original particle distributions and block- to lapillized fragments typically sediment within a few tens of kilometres from vent [Fig. 1 and Houghton et al. (1996, unpublished data)].

## Volume calculation

The volume of tephra-fall deposits is an important parameter in establishing the magnitudes of eruptions and in assessing risk and vulnerability. However, the calculation of volume is not straightforward because of several complications. These include (1) non-linearity of the functions linking thickness and area, (2) a general scarcity of data especially for prehistorical deposits, (3) lack of distal data points due to erosion or where distal tephra mainly falls into the sea, and (4) few very proximal points due to burial or vent collapse or inaccessibility. Such limitations in field data require extrapolation and interpolation and, hence, some assumption about thickness-area relationships. Unfortunately, a reliable and standard approach for the volume calculation of tephra-fall deposits is still not available, and several field-based (e.g. Fierstein and Hildreth 1992; Hildreth and Drake 1992; Scasso et al. 1994) and numerical studies (e.g. Bursik et al. 1992; Sparks et al. 1992; Bonadonna et al. 1998) have shown that methods based on the exponential decay of

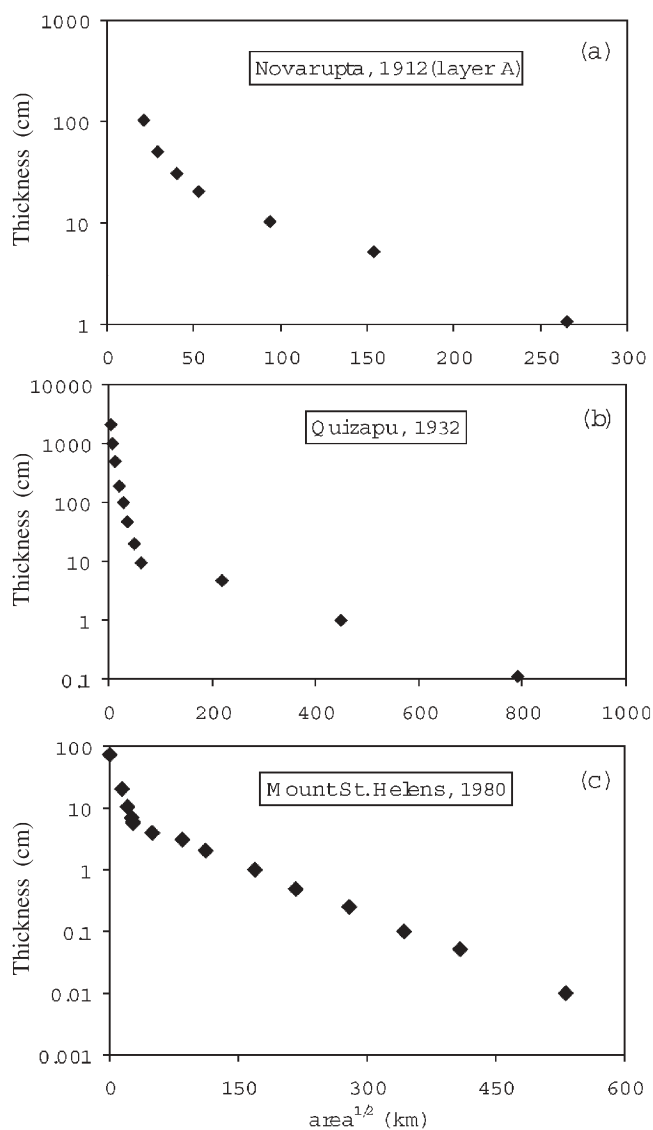
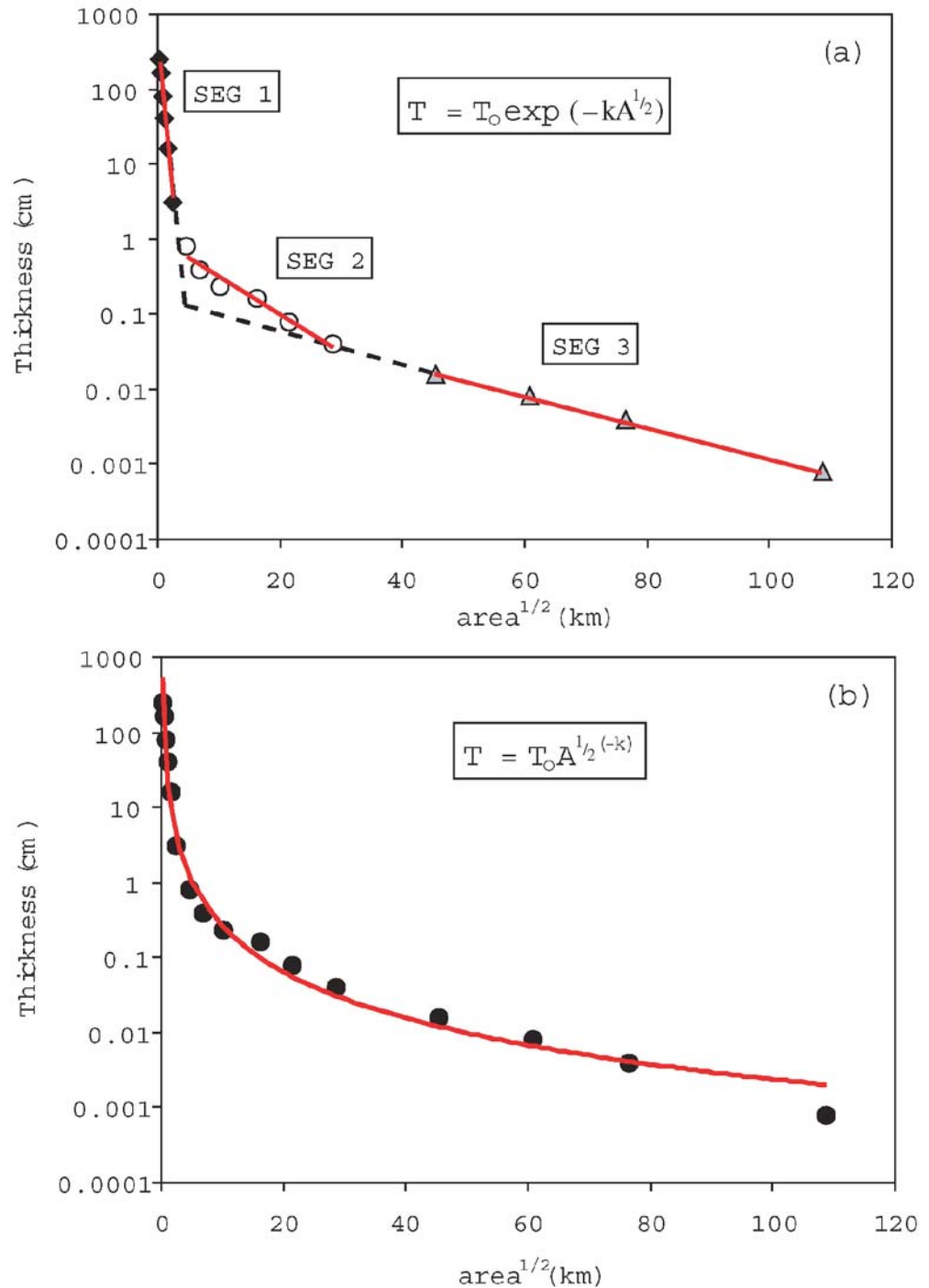


**Fig. 6** Semi-log plots of thickness vs  $(area)^{1/2}$  for tephra-fall deposits from **a** Novarupta, 1912 eruption (layer A; Hildreth and Drake 1992), **b** Quizapu, 1932 eruption (Fierstein and Hildreth 1992) and **c** Mt St Helens, 18 May 1980 eruption (Sarna-Wojcicki et al. 1981)

deposit thickness away from the vent (e.g. Pyle 1989; Fierstein and Nathenson 1992) can significantly underestimate the total volume, particularly for eruptions that produce a significant amount of fine ash. In fact, several of the best preserved tephra-fall deposits do not show a simple exponential thinning (e.g. Sarna-Wojcicki et al. 1981; Fierstein and Hildreth 1992; Hildreth and Drake 1992), and are approximated by two or more straight-line segments on a semi-log plot of thickness vs  $(area)^{1/2}$  (Fig. 6).

**Fig. 7** Semi-log plots of thickness vs  $(\text{area})^{1/2}$  for the Ruapehu deposit showing **a** exponential (red segments) and **b** power-law best fits (red curve). Three segments can describe the exponential fit, with  $R^2=0.997$ ,  $0.966$  and  $0.999$ , respectively. The power-law best fit gives a  $R^2=0.986$ . The dashed line indicates the extrapolation of the most proximal and most distal exponential segments (SEG 1 and SEG 3)



Exponential method applied to deposits showing one or more breaks-in-slope

The Ruapehu deposit can be approximated by a minimum of three segments on a semi-log plot of thickness vs  $(\text{area})^{1/2}$ , with breaks-in-slope at 3 and 29 km (Fig. 7a). Field data investigated in this paper were originally measured as mass per unit area (Houghton et al. 1996, unpublished data), which is the ideal technique to sample tephra-fall deposits wherever possible. However, old de-

posits are typically described by thickness values due to sampling difficulties in measuring mass per unit area. In order to present a general method to determine deposit volume, Ruapehu values of mass per unit area were divided by the measured deposit bulk density and converted to thickness. Volume calculations done on both data sets and corresponding thinning trends do not vary significantly because the variation of deposit bulk density with distance from vent was accounted for (Houghton et al. 1996, unpublished data).

To calculate the volume of a tephra-fall deposit on a semi-log plot of thickness vs (area)<sup>1/2</sup>, two main approaches have been used. Pyle (1989, 1990) made use of the assumption of elliptical and circular isopachs. Fierstein and Nathenson (1992) extended this approach to derive a similar result that is independent of the shape of isopachs (i.e. influence of wind advection). The volume integral  $V$  (m<sup>3</sup>) is:

$$V = \int_0^{\infty} T dA, \quad (1)$$

where  $A$  (m<sup>2</sup>) is the total area enclosed by the isopach line of thickness  $T$  (m). For the case of exponential thinning:

$$T = T_0 \exp(-k\sqrt{A}), \quad (2)$$

where  $T_0$  is the maximum thickness and  $k$  is the slope on plots of  $\ln(\text{thickness})$  vs (area)<sup>1/2</sup>. Changing variables and substituting Eq. (2) in Eq. (1) for the line segments before and after the break-in-slope, both Pyle (1990) and Fierstein and Nathenson (1992) derived a formula for volume in the case of one inflection point.

However, several deposits show more than one break-in-slope on a semi-log plot of thickness vs (area)<sup>1/2</sup> [e.g. Hekla 1947 (Thorarinsson 1967); Hudson 1991 (Scasso et al. 1994); Novarupta 1912 (Fierstein and Hildreth 1992); Quizapu 1932 (Hildreth and Drake 1992)], therefore a general formula is more appropriate. The calculation of the volume of tephra-fall deposit in case of  $n$  line segments (and hence  $(n-1)$  breaks-in-slope) can be obtained by integrating Eq. (2) for each of the  $n$  segments:

$$\begin{aligned} V = & \frac{2T_1 T_0}{k_1^2} + 2T_1 T_0 \left[ \frac{k_2 B S_1 + 1}{k_2^2} - \frac{k_1 B S_1 + 1}{k_1^2} \right] \exp(-k_1 B S_1) \\ & + 2T_2 T_0 \left[ \frac{k_3 B S_2 + 1}{k_3^2} - \frac{k_2 B S_2 + 1}{k_2^2} \right] \exp(-k_2 B S_2) + \dots \\ & + 2T(n-1) T_0 \left[ \frac{k_n B S_{(n-1)} + 1}{k_n^2} \right. \\ & \left. - \frac{k_{(n-1)} B S_{(n-1)} + 1}{k_{(n-1)}^2} \right] \exp(-k_{(n-1)} B S_{(n-1)}) \end{aligned} \quad (3)$$

where  $T_n$ ,  $-k_n$  and  $B S_n$  are the intercept, slope and break-in-slope of the line segment  $n$ . This formula applied to Fig. 7a with  $n=3$  gives a total bulk volume of  $4.0 \times 10^6$  m<sup>3</sup> for the Ruapehu deposit.

#### Power-law method

Ruapehu data show an equally good agreement with a power-law relationship between thickness and (area)<sup>1/2</sup> (Fig. 7b) with:

$$T = T_{pl} \sqrt{A}^{(-m)}, \quad (4)$$

where  $T_{pl}$  is a constant and  $m$  is the power-law coefficient. Changing variables and substituting Eq. (4) in Eq. (1), the following function is obtained:

$$V = \left[ 2T_{pl} \frac{\sqrt{A}^{(2-m)}}{2-m} \right]_0^{\infty}. \quad (5)$$

To prevent values of Eq. (5) becoming infinite when  $\sqrt{A} = 0$ , and when  $\sqrt{A} = \infty$ , two arbitrary integration limits  $B$  and  $C$  need to be defined. Thus, Eq. (5) becomes:

$$V = \frac{2T_{pl}}{2-m} (C^{(2-m)} - B^{(2-m)}). \quad (6)$$

For the Ruapehu deposit,  $B$  is chosen as the distance of the calculated maximum thickness, i.e. value of  $\sqrt{A}$  in Eq. (4) when  $T = T_0$  in Eq. (2):

$$B = \left( \frac{T_0}{T_{pl}} \right)^{\left(-\frac{1}{m}\right)}. \quad (7)$$

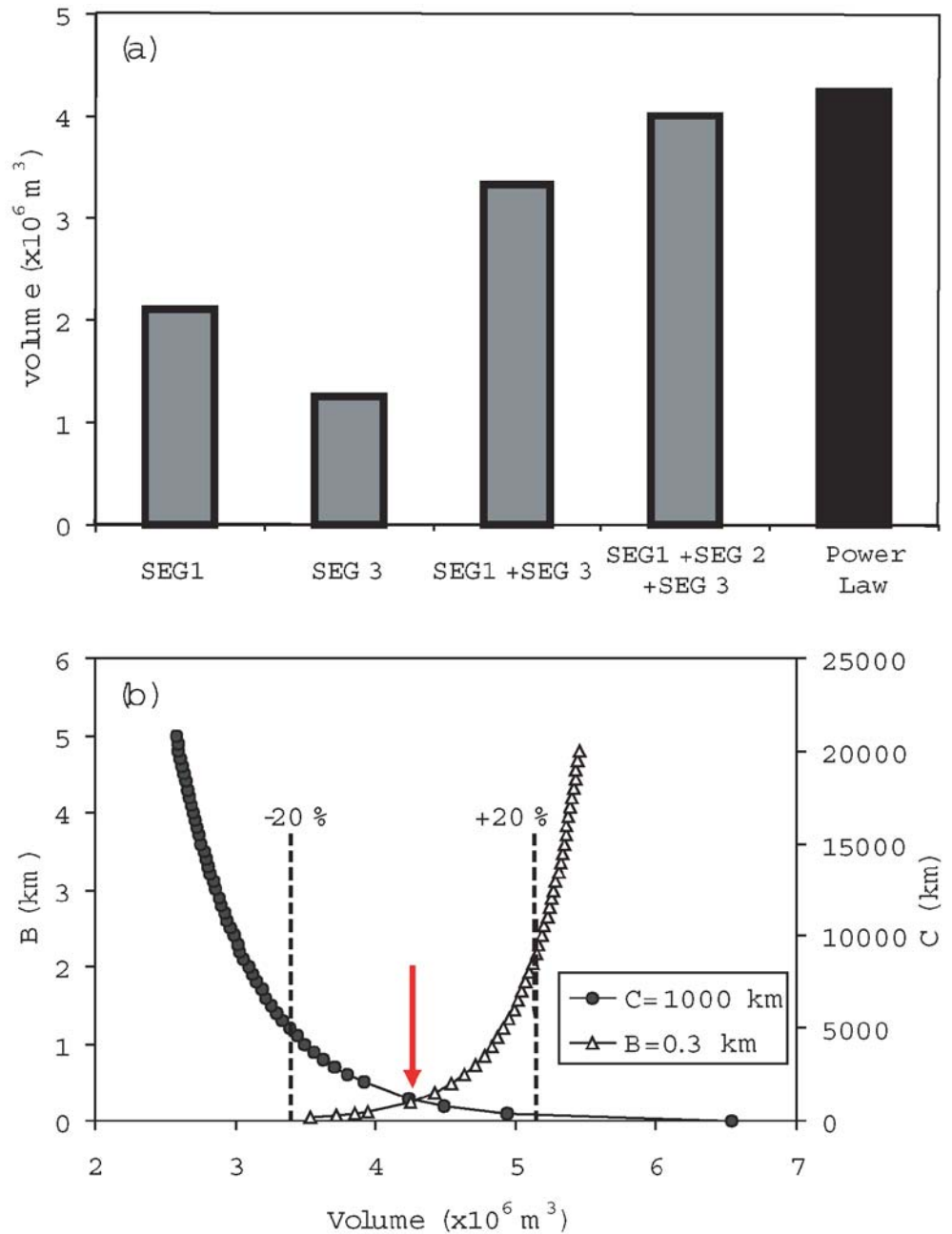
where  $T_0$  is the maximum thickness, and  $T_{pl}$  and  $m$  are the power-law constant and coefficient in Eq. (4).  $C$  is chosen as the downwind limit of significant volcanic-cloud spreading as shown by satellite images (Prata and Grant 2001). Thus,  $B=0.3$  km and  $C=1,000$  km.  $C$  extends about 700 km beyond the mappable limit of the deposit on land (Fig. 1). Equation (6) applied to the plot in Fig. 7b with these integration limits gives a bulk volume of  $4.2 \times 10^6$  m<sup>3</sup>, very similar to the result obtained by integrating three exponential segments (i.e.  $4.0 \times 10^6$  m<sup>3</sup>; Fig. 7a).

#### Investigations on exponential and power-law methods and comparison of results

Most deposits of tephra fall are not as well preserved as the Ruapehu deposit. The corresponding data sets are often smaller, and, if plotted on a semi-log plot of thickness vs (area)<sup>1/2</sup>, the data may not be sufficient to allow an accurate thinning trend to be recognised. If all tephra-fall deposits were perfectly preserved and not affected by secondary processes (e.g. particle aggregation, convective instabilities), they would be expected to plot as a curve on semi-log plots of thickness vs (area)<sup>1/2</sup>, as suggested by numerical studies (e.g. Sparks et al. 1992; Bonadonna and Phillips 2003). Therefore, the Ruapehu data set is used here to investigate the accuracy of the exponential and power-law methods when applied to small and biased data sets.

Figure 8a shows the comparison of volumes obtained integrating one, two or three exponential line segments in Fig. 7a and the power-law fit in Fig. 7b. The use of only one or two of the exponential line segments significantly underestimates the volume (between 70 and 20% of the volume obtained integrating all three segments; Fig. 8a). The sensitivity of the power-law technique to the choice of the integration limits  $B$  and  $C$  is also investigated (Fig. 8b). Considering a bulk volume of  $4.2 \times 10^6$  m<sup>3</sup> as the

**Fig. 8 a** Comparison of volumes calculated integrating one, two or three exponential segments and the power-law fit in Fig. 7b Comparison of volumes obtained integrating the power-law fit using different integration limits  $B$  and  $C$ . *Black dots* indicate volumes calculated by varying  $B$  between 0.01 and 5 km with  $C=1,000$  km. *White triangles* indicate volumes calculated by varying  $C$  between 200 and 20,000 km with  $B=0.3$  km. The best volume estimate is indicated by the *red arrow* (i.e.  $4.2 \times 10^6 \text{ m}^3$ ; **a**). *Dashed lines* indicate an error of 20 vol%

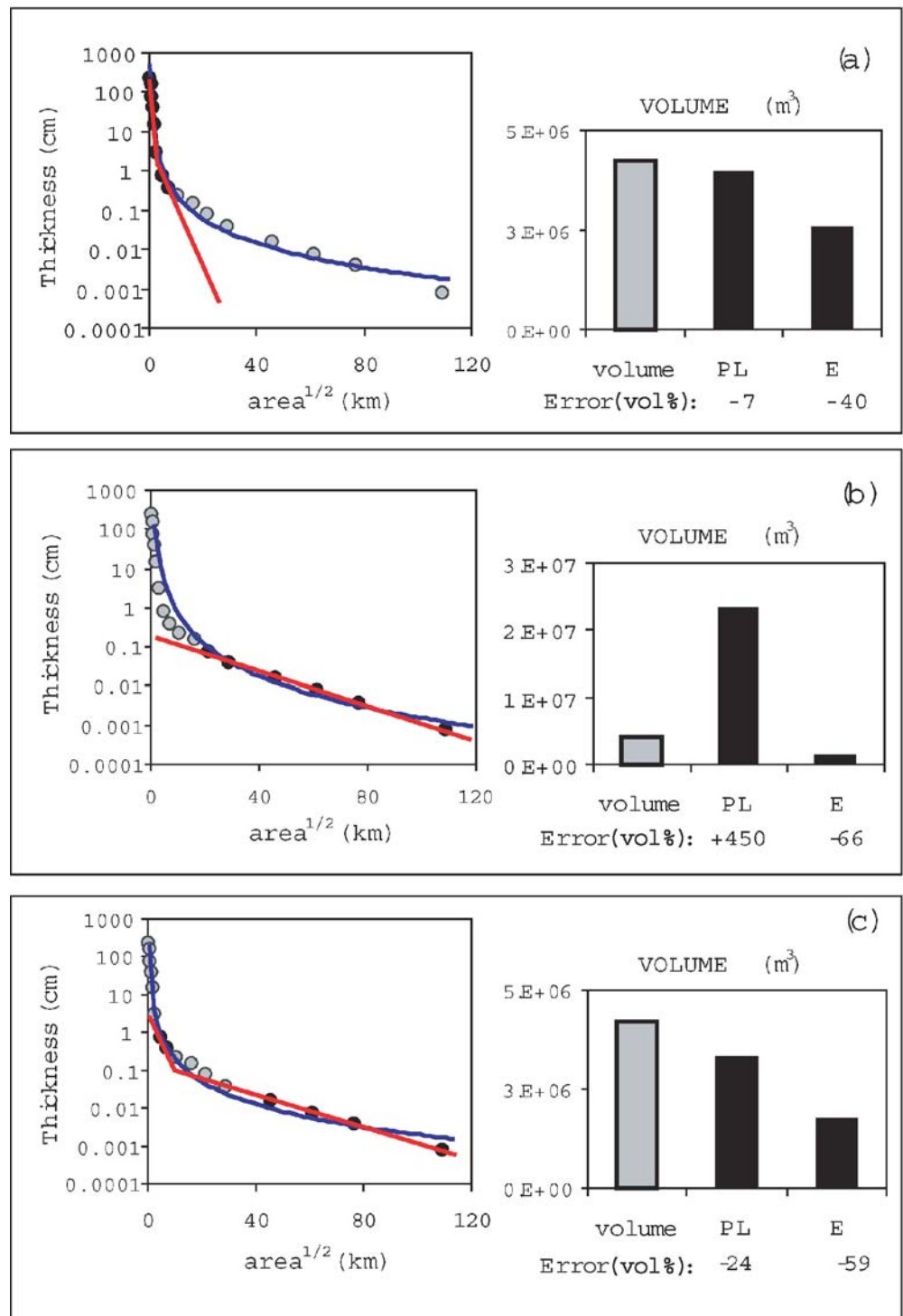


best estimate for Ruapehu (with  $B=0.3$  km and  $C=1,000$  km for the reasons described above; Fig. 8a), errors are within 20%vol for volumes obtained by integration of the power-law fit with  $C=1,000$  km and  $B < 1$  km, and  $B=0.3$  km and  $200 < C < 8,000$  km (Fig. 8b).

Exponential (E) and power-law (PL) fits were also investigated for three subsamples: a few data points in a narrow interval (i.e. 0–30 km distance from vent, corresponding to  $(\text{area})^{1/2}=0-7$  km in Fig. 9a, and 46–250 km distance from vent, corresponding to  $(\text{area})^{1/2}=21-109$  km in Fig. 9b), and a selection of medial and distal data points non-uniformly distributed (i.e. between 15–30 and 150–250 km, corresponding to  $5 < (\text{area})^{1/2} < 7$  km and  $45 < (\text{area})^{1/2} < 109$  km in Fig. 9c). Results of volume cal-

culations using the two methods are shown in Fig. 9. Note that for most subsamples the volumes are underestimated by between 7–70 vol% using both techniques, with the exception of the distal-data subsample that gives the largest discrepancy with an overestimation of about 450 vol% of the actual volume by integrating the power-law fit. The smallest discrepancy obtained in this test is given by the power-law method applied to the proximal-data subsample (i.e. -7vol%; Fig. 9a). For the subsample comprising medial- and distal-data points, the discrepancy is about -24 and -59 vol% for the power-law and exponential method, respectively. The two integration limits  $B$  and  $C$  used in the integration of the power-law

**Fig. 9** Comparison of volume-calculation methods for three different subsamples of the Ruapehu data. **a** Proximal data,  $(\text{area})^{1/2} = 0.2\text{--}7$  km, **b** distal data  $(\text{area})^{1/2} = 21\text{--}109$  km and **c** medial and distal data,  $5 < (\text{area})^{1/2} < 7$  km and  $45 < (\text{area})^{1/2} < 109$  km. Grey circles on plots of thickness vs  $(\text{area})^{1/2}$  represent the complete data set, whereas black circles represent the three sub-samples analysed. Red segments and blue curves represent the exponential and power-law fits, respectively, for the three sub-samples. The power-law fit is integrated between  $B=0.3$  km and  $C=1,000$  km. Corresponding relative error is also calculated for the exponential (E) and power-law (PL) methods (black bars) relatively to the volume obtained using the complete data set (grey bar, i.e.  $4.2 \times 10^6$  m<sup>3</sup>, in Fig. 8)



fits in Fig. 9 are the same used for the integration of the whole data set (i.e.  $B=0.3$  km and  $C=1,000$  km).

Table 2 shows a comparison between bulk volumes of seventeen tephra-fall deposits calculated by the power-law and the exponential methods. The choice of integration limits  $B$  and  $C$  for old deposits is difficult and arbitrary. In this test, the power-law fit was integrated between  $B = 0.3$  km and  $C = 1,000$  km, consistent with the Ruapehu study. Results from other authors based on other

techniques are also shown: the crystal-concentration method (Walker 1980), the method based on Log-Log plots with two straight-lines approximation (Rose et al. 1973), and the trapezoidal rule (Froggatt 1982). The crystal-concentration method was developed to deal with tephra-fall deposits for which the data availability on land is poor, e.g. Taupo (Walker 1980). This is mainly based on the assumption that large pumices are representative of the original magma and so they can be used to determine

**Table 2** Volume estimates. Data to the right of 'Exp' are estimates made by other authors (shaded columns). *Data*: number of isopach contours available; *min.* and *max. area*<sup>1/2</sup>: values of minimum and maximum (area)<sup>1/2</sup> covered by the data available; *m*: power-law coefficient in power-law fit, Eq. 4); *PL*: power law method (integration limits: *B*=0.3 km and *C*=1,000 km for all deposits); *EXP*: exponential method (Pyle 1989; Fierstein and Nathenson 1992) (number of segments used in the calculation is in bracket); *Cryst.*: crystal-concentration method (Walker 1980); *Log-Log*: two line-segment approximation based on a log-log scale (Rose et al. 1973); *Trap.*: trapezoidal rule based on a linear scale (Froggatt 1982); *Others*: specific methods used for individual deposits: <sup>a</sup>application of the trapezoidal rule to an extrapolation of thickness data based

on the tephra-fall deposit from Quizapu 1932 (Hudson); <sup>b</sup>direct measurements of isopach area and thickness inside the 0.5-mm contour (MSH); <sup>c</sup>modification of the exponential method accounting for tephra-fall mixing within different layers (Novarupta); <sup>d</sup>exponential method applied to an extrapolation of thickness data based on the tephra-fall deposit from Taupo 186 A.D. (Tarawera). References: Askja D (Sparks et al. 1981); Fogo (Walker and Croasdale 1971); Hatepe (Walker 1981); Hekla (Thorarinsson 1967); Hudson (Scasso et al. 1994); Minoan eruption (Pyle 1990); Mount St. Helens (Sarna-Wojcicki et al. 1981); Novarupta (Fierstein and Hildreth 1992); Quizapu (Hildreth and Drake 1992); Santa Maria (Williams and Self 1983); Tarawera (Walker et al. 1984); Taupo (Walker 1980); Vesuvius (Sigurdsson et al. 1985)

	Data	Min. area <sup>1/2</sup> (km)	Max. area <sup>1/2</sup> (km)	<i>m</i>	Volume (km <sup>3</sup> )					
					PL	EXP	Cryst.	Log-Log	Trap.	Others
Askja D (1875)	6	1.4	52.0	1.14	2.6	0.3 (2)	-	-	0.6	-
Fogo (1563)	5	1.4	14.9	1.14	11.6	0.4 (1)	-	-	-	-
Hatepe (186 A.D.)	7	12.2	96.3	1.42	2.9	1 (2)	6.0	-	-	-
Hekla (1947)	11	3.9	264.6	2.23	0.3	0.2 (3)	-	-	0.2	-
Hudson (1991)	10	6.9	151.9	1.36	7.0	6.9 (3)	-	-	-	7.6 <sup>a</sup>
Minoan (3.6 ka B.P.)	7	0.8	438.1	0.68	87.4	43.8 (2)	-	-	28.0	-
MSH (18 May 1980)	15	0.7	531.8	1.27	1.3	1.1 (2)	-	-	-	1.4 <sup>b</sup>
Novarupta, A (1912)	7	21.4	265.0	1.66	9.0	5.2 (2)	-	-	-	6.1 <sup>c</sup>
Novarupta, B (1912)	6	5.9	202.1	1.26	6.4	2.5 (2)	-	-	-	2.7 <sup>c</sup>
Novarupta, CDE (1912)	8	2.9	163.4	1.69	4.5	2.7 (3)	-	-	-	4.8 <sup>c</sup>
Novarupta, FGH (1912)	10	3.9	332.3	1.24	13.2	7.5 (3)	-	-	-	3.4 <sup>c</sup>
Quizapu (1932)	11	6.4	790.6	1.88	12.4	9.5 (3)	-	-	-	-
Ruapehu (17 June 1996)	16	0.2	109.0	2.05	0.004	0.004 (3)	-	-	-	-
Santa Maria (1902)	6	6.0	151.0	0.77	61.8	9.2 (1)	20.0	8.2	-	-
Tarawera (1886)	6	8.9	41.4	2.23	1.8	0.5 (1)	-	-	-	2.0 <sup>d</sup>
Taupo (186 A.D.)	5	14.3	118.6	1.18	29.9	6.7 (1)	24.0	-	-	-
Vesuvius, GP (79 A.D.)	4	4.0	44.0	0.71	51.0	2 (2)	-	6.4	-	-

the crystal/glass ratio. However, the crystal content of pumices in some tephra-fall deposits is widely variable, making this method difficult to apply. The method based on the Log-Log scale was developed to deal with the non-linearity of thickness-distance data. However, the Log-Log plots do not reduce the curvature of a thickness-distance relationship, making the extrapolation to distal area difficult to compute. Finally, the trapezoidal rule based on a linear scale is very sensitive to the availability of data and does not allow any extrapolation to distal areas. Results from some specific techniques used for some deposits are also shown. The power-law coefficient *m* for tephra-fall deposits varies between about 0.7 and 2.2 (Table 2).

The absolute reliability of volume estimates is difficult to constrain without access to data sets equally as complete as the Ruapehu one and, therefore, our investigations (Fig. 9) cannot be used as a general rule for all tephra-fall deposits. However, a relation between number of isopach contours available and quality of volume estimates can be seen in Table 2. In fact, exponential and power-law techniques give similar results when a large data set is available, with three exponential segments defined (i.e. 10–16 isopach contours: Hekla, Hudson, MSH, Quizapu, Ruapehu; Table 2). The power-law extrapolation gives significantly higher values than the exponential technique, when the data set is poor, i.e. with only one or two exponential segments defined (e.g. 4 to 7

isopach contours: Fogo, Minoan, Santa Maria, Taupo, Vesuvius; Table 2).

The main discrepancies between power-law and exponential techniques are shown by those deposits with a power-law coefficient  $m < 1$  (i.e. Minoan, Santa Maria and Vesuvius deposits; Table 2) and, therefore, by those deposits that are characterised by a gradual thinning. Typically, this is true for large Plinian eruptions that generate extended tephra-fall deposits (e.g. Walker 1981b). Equation (6) shows that the integration of the power-law fit for deposits with  $m < 2$  is very sensitive to the choice of the integration limits and, therefore, is more problematic. As a conclusion, the integration of the power-law fit when  $m \geq 2$  (deposits with rapid thinning) is more reliable because it is not very sensitive to the integration limits (e.g. Hekla, Ruapehu, Tarawera; Table 2). This is also confirmed by the sensitivity tests done on the integration limits for Ruapehu (Fig. 8b).

#### Discussion on volume calculations

In a similar fashion to the whole-deposit grain-size evaluation, volume calculations are very dependent on availability of data. Several authors have tried to provide reliable methods of extrapolation of existing data by different techniques, but the typically limited availability of field data makes the choice of empirical laws for extrapolation subjective and potentially misleading. Vol-

umes of tephra-fall deposits calculated in this fashion have then been often underestimated and have often needed to be revised using new available techniques, e.g. Minoan eruption, 3.6 ka B.P. (Pyle 1990).

A new method for volume calculation by integration of the power-law fit was presented in this paper and investigated together with existing techniques. The power-law technique has the advantage of fitting the available data without having to introduce any interpretation on the choice of segments as for the exponential technique, and providing for the gradual thinning of tephra-fall deposits in distal area. However, this technique presents some problems mainly because finite integration limits have to be chosen.

The power-law and exponential techniques were tested using 17 tephra-fall deposits and compared with other popular techniques showing the following results (Fig. 9 and Table 2). First, when at least three segments can be defined on a semi-log plot of thickness vs (area)<sup>1/2</sup>, the exponential and power-law methods give very similar estimates for tephra-fall volumes, with the former being easier to apply using Eq. (3) (Table 2). Second, if distal data are missing, the power-law extrapolation gives better results; however, if proximal data are missing, both techniques fail to give a reliable good estimate, with the power-law technique giving the largest error (Fig. 9). Third, the integration of the power-law fit is more reliable when the power-law coefficient  $m$  is  $\geq 2$  because, in such a case, this technique is less sensitive to the choice of the integration limits (Table 2). More constraints on actual volumes by other derivations are needed to give a final assessment on calculations of tephra-fall volumes.

Our study shows that volume estimates can vary widely depending on whether a power-law or exponential fit is used. Numerical studies (e.g. Bonadonna et al. 1998) favour the power-law approach because tephra-fall deposits consist of particles with different Reynolds number, and models are better described through power laws, particularly when data from distal areas are available. Some well-preserved tephra-fall deposits are also well described by a power-law fit (e.g. Ruapehu, 17 June 1996; Hudson 1991; Novarupta 1912, all layers). However, some well-preserved tephra fall deposits cannot be accurately described by a power-law fit (e.g. Mount St. Helens, 18 May 1980) because they were influenced by particle-aggregation processes that significantly affect the thinning trend making fine particles fall in the intermediate and turbulent regimes (Bonadonna and Phillips 2003). It is interesting to note that, even though the field data for Mount St. Helens 1980 do not show a power-law thinning (Fig. 6c), the application of the power-law method still gives good volume results (Table 2). This can be due to the fact that particle aggregation affected the thinning trend in medial area, but that the power-law thinning represents the deposit as if it had not been affected by particle aggregation. In all situations, particle sedimentation in proximal and distal areas is governed by different settling regimes, the distal deposition being controlled by low-Reynolds number particles (e.g. Rose

1993; Bonadonna et al. 1998). Therefore, there is no reason to suppose that distal deposition should bear any simple or systematic relation to proximal deposition. This is also supported by the volume investigations in Fig. 9 that show that the power-law approach gives good results only when at least some proximal and some distal data are available in order to constrain the actual deposit-thinning curvature. If only distal data are available, also the power-law approach fails to give a good estimate of the actual deposit volume. As a result, both exponential and power-law fit are to be used cautiously, bearing in mind that tephra-fall deposit thinning cannot be easily extrapolated by a simple curve fit based on the available data, if nothing is known about either the proximal or distal thinning.

## Conclusions

Given the large data set of the tephra-fall deposit from the 17 June 1996 eruption of Ruapehu some investigations on the methods of calculating total grain-size distribution and volume were made. A new method to calculate the total grain-size distribution (i.e. Voronoi tessellation) and a new method to calculate tephra-fall volumes (i.e. integration of power-law fit) are presented and compared with existing techniques.

In terms of grain-size evaluation for the whole deposit we can conclude that:

- The most common techniques for calculation of the total grain-size distribution of tephra-fall deposits are (1) weighted average of sample grain-size distribution for all samples over the whole deposit, and (2) various types of arbitrary sectorisation of tephra-fall deposits. The first technique cannot deal with deposits with non-uniform distributions of data, whereas the second is biased due to the arbitrary choice of sectors.
- The Voronoi tessellation technique provides a better statistical method that deals with non-uniform data sets without introducing arbitrary sectors. The use of such a technique would make comparisons amongst different tephra-fall deposits analysed by different authors more consistent.
- All existing techniques to calculate total grain-size distribution of an eruption give only apparent distributions if the data set is small. However, the sensitivity of the analysis depends on the original sorting of the particle distribution and the style and intensity of the corresponding eruption.
- The total grain-size distribution of the Ruapehu deposit calculated by Voronoi Tessellation shows a Gaussian distribution with 99.9 wt% of the deposit consisting of particles with diameter between 256  $\mu\text{m}$  and 1  $\mu\text{m}$ . Two lognormal sub-populations with modes at 8 and 1 mm could also be fitted, with particle fraction of about 40 and 60 wt%, respectively.  $Md_\phi$  is  $-0.8\phi$  and  $\sigma_\phi$  is 2.4.

In terms of calculations for tephra-fall volumes we can conclude that:

- The Ruapehu large data set supports the idea that thinning of tephra-fall deposits cannot be described by a simple exponential decay: at least three distinct exponential segments can be defined and a power-law trend also gives a good fit. Integrations of both fits give similar volumes of about  $4 \times 10^6 \text{ m}^3$ .
- Integration of <3 exponential segments significantly underestimates the volume of tephra-fall deposits, especially when distal data are missing. Therefore, for many prehistoric deposits where only proximal and medial data are available, large uncertainties in volume estimates are expected.
- The integration of the power-law fit gives similar volume estimates to the integration of at least three exponential segments, but gives better results than the exponential techniques when distal data are missing.
- Although power-law fits provide a good approximation to well-preserved deposits and are consistent with theoretical models, this method is also problematic because (1) integration limits have to be chosen and (2) it cannot reproduce the proximal thinning when proximal and/or medial data are missing.
- Integration of the power-law fit is not very sensitive to the choice of the integration limits when the power-law coefficient  $m \geq 2$ , but it is very sensitive when  $m \ll 2$ , i.e. for large tephra-fall deposits.
- Proximal deposition is governed by high Reynolds number particles and distal deposition is governed by low Reynolds number particles, and so there is no theoretical simple relation between proximal and distal thinning. Thus, any extrapolation based on empirical fitting of poor data sets related to only one of these regimes is likely to be problematic and unsafe, with large uncertainties.

**Acknowledgements** The authors are grateful to Steve Carey, Dave Pyle and Steve Sparks for constructive review of the manuscript and to Jon Blower for helpful discussion on the application of the Voronoi tessellation method. The Ruapehu data set was collected with the assistance of a large number of New Zealand colleagues including Thor Thordarson, Mike Rosenberg, Colin Wilson, David Johnston, Rod Burt, Bruce Christiansen, Will Esler, Barbara Hobden, Katy Hodgson, Zinzuni Jurado-Chichay, Barry Lowe, Richard Smith, Jeff Willis and Vince Udy. This work was supported by an EC Marie Curie PhD Fellowship at Bristol University (UK), by NSF-EAR-0310096, NSF-EAR-012579 and by several grants by the New Zealand Foundation for Research and Sciences Technology.

## References

- Barberi F, Macedonio G, Pareschi MT, Santacroce R (1990) Mapping the tephra fallout risk: an example from Vesuvius, Italy. *Nature* 344:142–144
- Blower JD, Keating JP, Mader HM, Phillips JC (2003) The evolution of bubble size distributions in volcanic eruptions. *J Volcanol Geotherm Res* 120(1–2):1–23
- Bohm G, Galuppo P, Vesnaver A (2000) 3D adaptive tomography using Delaunay triangles and Voronoi polygons. *Geophys Prospect* 48:723–744
- Bonadonna C, Phillips JC (2003) Sedimentation from strong volcanic plumes. *J Geophys Res* 108(B7):2340–2368
- Bonadonna C, Ernst GGJ, Sparks RSJ (1998) Thickness variations and volume estimates of tephra fall deposits: the importance of particle Reynolds number. *J Volcanol Geotherm Res* 81:173–187
- Bonadonna C, Macedonio G, Sparks RSJ (2002a) Numerical modelling of tephra fallout associated with dome collapses and Vulcanian explosions: application to hazard assessment on Montserrat. In: Druitt TH, Kokelaar BP (eds) *The eruption of Soufrière Hills Volcano, Montserrat, from 1995 to 1999. Memoir, Geological Society, London*, pp 517–537
- Bonadonna C, Mayberry GC, Calder ES, Sparks RSJ, Choux C, Jackson P, Lejeune AM, Loughlin SC, Norton GE, Rose WI, Ryan G, Young SR (2002b) Tephra fallout in the eruption of Soufrière Hills Volcano, Montserrat. In: Druitt TH, Kokelaar BP (eds) *The eruption of Soufrière Hills Volcano, Montserrat, from 1995 to 1999. Memoir, Geological Society, London*, pp 483–516
- Brown KQ (1979) Voronoi Diagrams from Convex Hulls. *Inform Proc Lett* 9(5):223–228
- Bursik MI, Sparks RSJ, Gilbert JS, Carey SN (1992) Sedimentation of tephra by volcanic plumes: I. Theory and its comparison with a study of the Fogo A Plinian deposit, Sao Miguel (Azores). *Bull Volcanol* 54:329–344
- Carey SN, Sigurdsson H (1982) Influence of particle aggregation on deposition of distal tephra from the May 18, 1980, eruption of Mount St-Helens volcano. *J Geophys Res* 87(B8):7061–7072
- Connor CB, Hill BE, Winfrey B, Franklin NM, La Femina PC (2001) Estimation of volcanic hazards from tephra fallout. *Natural Hazards Rev* 2:33–42
- Cronin SJ, Hedley MJ, Neall VE, Smith RG (1998) Agronomic impact of tephra fallout from the 1995 and 1996 Ruapehu Volcano eruptions, New Zealand. *Environ Geol* 34:21–30
- Dupuis F, Sadoc JF, Mornon JP (2004) Protein secondary structure assignment through Voronoi tessellation. *Proteins-Structure Funct Bioinform* 55:519–528
- Duyckaerts C, Godefroy G (2000) Voronoi tessellation to study the numerical density and the spatial distribution of neurones. *J Chem Neuroanat* 20:83–92
- Fierstein J, Hildreth W (1992) The plinian eruptions of 1912 at Novarupta, Katmai National Park, Alaska. *Bull Volcanol* 54:646–684
- Fierstein J, Nathenson M (1992) Another look at the calculation of fallout tephra volumes. *Bull Volcanol* 54:156–167
- Froggatt PC (1982) Review of methods estimating rhyolitic tephra volumes; applications to the Taupo Volcanic Zone, New Zealand. *J Volcanol Geotherm Res* 14:1–56
- Gowda IG, Kirkpatrick DG, Lee DT, Naamad A (1983) Dynamic Voronoi Diagrams. *IEEE Trans Inform Theory* 29:724–731
- Haydon DT, Pianka ER (1999) Metapopulation theory, landscape models, and species diversity. *Ecoscience* 6:316–328
- Hildreth W, Drake RE (1992) Volcano Quizapu, Chilean Andes. *Bull Volcanol* 54:93–125
- Houghton BF, Wilson CJN (1998) Fire and water: the physical roles of water in caldera eruptions at Taupo and Okataina volcanic centres. *Water-Rock Interaction, Taupo, New Zealand*, pp 25–30
- Hurst AW, Turner R (1999) Performance of the program ASH-FALL for forecasting ashfall during the 1995 and 1996 eruptions of Ruapehu volcano. *New Zealand J Geol Geophys* 42:615–622
- Inman DL (1952) Measures for describing the size distribution of sediments. *J Sediment Petrol* 22:125–145
- Jasny (1988) Exploiting the insights from protein structure. *Science* 240:722–723
- Kaminski E, Jaupart C (1998) The size distribution of pyroclasts and the fragmentation sequence in explosive volcanic eruptions. *J Geophys Res-Solid Earth* 103(B12):29759–29779

- Klein R (1989) Concrete and abstract Voronoi diagrams. Springer Lecture Notes in Computer Science #400, Berlin Heidelberg New York
- Moore KR, Duffell H, Nicholl A, Searl A (2002) Monitoring of airborne particulate matter during the eruption of Soufrière Hills Volcano, Montserrat. In: Druitt TH, Kokelaar BP (eds) The eruption of Soufrière Hills Volcano, Montserrat, from 1995 to 1999. Memoir, Geological Society, London, pp 557–566
- Murrow PJ, Rose WI, Self S (1980) Determination of the total grain size distribution in a Vulcanian eruption column, and its implications to stratospheric aerosol perturbation. *Geophys Res Lett* 7:893–896
- Nelson RA (1979) Natural fracture systems: descriptions and classification. *Bull Am Assoc Petrol Geol* 63:2214–2219
- Okabe A, Boots B, Sugihara K (1992) Spatial tessellations: concepts and applications of Voronoi diagrams. Wiley, Chichester
- Parfitt EA (1998) A study of clast size distribution, ash deposition and fragmentation in a Hawaiian-style volcanic eruption. *J Volcanol Geotherm Res* 84:197–208
- Prata AJ, Grant IF (2001) Retrieval of microphysical and morphological properties of volcanic ash plumes from satellite data: application to Mt Ruapehu, New Zealand. *Q J R Meteorol Soc* 127:2153–2179
- Pyle DM (1989) The thickness, volume and grain-size of tephra fall deposits. *Bull Volcanol* 51:1–15
- Pyle DM (1990) New estimates for the volume of the Minoan eruption. In: Hardy DA (ed) *Thera and the Aegean World, III*. Thera Foundation, London, pp 113–121
- Pyle DM (1995) Assessment of the minimum volume of tephra fall deposits. *J Volcanol Geotherm Res* 69:379–382
- Rose WI (1993) Comment on another look at the calculation of fallout tephra volumes. *Bull Volcanol* 55:372–374
- Rose WI, Bonis S, Stoiber RE, Keller M, Bickford T (1973) Studies of volcanic ash from two recent Central American eruptions. *Bull Volcanol* 37:338–364
- Sarna-Wojcicki AM, Shipley S, Waitt JR, Dzurisin D, Wood SH (1981) Areal distribution thickness, mass, volume, and grain-size of airfall ash from the six major eruptions of 1980. *US Geol Surv Prof Pap* 1250:577–600
- Scasso R, Corbella H, Tiberi P (1994) Sedimentological analysis of the tephra from 12–15 August 1991 eruption of Hudson Volcano. *Bull Volcanol* 56:121–132
- Sigurdsson H, Carey S, Cornell W, Pescatore T (1985) The eruption of Vesuvius in A.D. 79. *Nat Geogr Res* 1:332–387
- Sparks RSJ, Wilson L, Sigurdsson H (1981) The pyroclastic deposits of the 1875 eruption of Askja, Iceland. *Phil Trans R Soc Lond* 229:241–273
- Sparks RSJ, Bursik MI, Ablay GJ, Thomas RME, Carey SN (1992) Sedimentation of tephra by volcanic plumes .2. Controls on thickness and grain-size variations of tephra fall deposits. *Bull Volcanol* 54:685–695
- Thorarinsson S (1967) The eruption of Hekla 1947–1948. *Vindindafélag Islendinga Reykjavik*
- Walker GPL (1980) The Taupo Pumice: product of the most powerful known (Ultraplinian) eruption? *J Volcanol Geotherm Res* 8:69–94
- Walker GPL (1981a) Characteristics of two phreatoplinian ashes, and their water-flushed origin. *J Volcanol Geotherm Res* 9:395–407
- Walker GPL (1981b) Plinian eruptions and their products. *Bull Volcanol* 44 223–240
- Walker GPL (1981c) The Waimihia and Hatepe plinian deposits from the rhyolitic Taupo Volcanic Centre. *NZ J Geol Geophys* 24:305–324
- Walker GPL, Croasdale R (1971) Two plinian-type eruptions in the Azores. *J Geol Soc Lond* 127:17–55
- Walker GPL, Self S, Wilson L (1984) Tarawera, 1886, New Zealand — a basaltic Plinian fissure eruption. *J Volcanol Geotherm Res* 21:61–78
- Wen S, Rose WI (1994) Retrieval of sizes and total masses of particles in volcanic clouds using AVHRR bands 4 and 5. *J Geophys Res* 99:5421–5431
- Wilkinson BH, Drummond CN, Diedrich NW, Rothman ED (1999) Poisson processes of carbonate accumulation on Paleozoic and Holocene platforms. *J Sediment Res* 69:338–350
- Williams SN, Self S (1983) The October 1902 Plinian eruption of Santa Maria volcano, Guatemala. *J Volcanol Geotherm Res* 16:33–56
- Wohletz KH, Sheridan MF, Brown WK (1989) Particle-size distributions and the sequential fragmentation/transport theory applied to volcanic ash. *J Geophys Res* 94(B11):15703–15721
- Zhan XJ, Troy JB (2000) Modeling cat retinal beta-cell arrays. *Visual Neurosci* 17:23–39